

Hidden persistent spin texture in bulk crystals

Shan Guan¹ and Jun-Wei Luo^{1, 2, 3, *}

¹*State Key Laboratory of Superlattices and Microstructures, Institute of Semiconductors, Chinese Academy of Sciences, Beijing 100083, China*
²*Center of Materials Science and Optoelectronics Engineering, University of Chinese Academy of Sciences, Beijing 100049, China*
³*Beijing Academy of Quantum Information Sciences, Beijing 100193, China*

Exploring hidden effects that have been overlooked given the nominal global crystal symmetry but are indeed visible in solid-state materials has been a fascinating subject of research recently. Here, we introduce a novel type of hidden persistent spin texture (HPST) in nonmagnetic bulk crystals consisting of a pair of real-space sectors. In these crystals, the doubly degenerate bands formed in the momentum space can exhibit a uniform spin configuration with opposite spin orientations, which are spatially separated in the paired sectors. Interestingly, we find that such a type of spin texture can be hidden in both centrosymmetric and non-centrosymmetric materials. We further demonstrate the important role of nonsymmorphic twofold screw-rotational symmetry played in the formation of HPST. Moreover, two representative material examples, i.e., centrosymmetric WSe₂ and noncentrosymmetric BaBi₄O₇, are identified to show HPST via first-principles calculations. Our finding thus not only opens new perspectives for hidden spin polarization research but also significantly broadens the range of materials towards spintronics applications.

Introduction. Since the discovery of hidden spin polarization in centrosymmetric crystals [1], the past few years have witnessed a surge of interest in both the theoretical and experimental exploration of hidden physical effects in condensed matter systems [2–5], which refer to that the said effect indeed exists and can be observed arising from the local site symmetry whereas the global crystal symmetry would seemingly forbid it [6, 7]. A variety of hidden-like effects, including intrinsic circular polarization [8], hidden orbital polarization [9], hidden Berry curvature [10], unconventional superconductor [11, 12], layer-valley coupling [13], hidden anomalous Hall effect [14], are revealed. These findings considerably enrich the material candidates for studying the target effects that have been limited to systems with certain global crystal symmetry before, and provide new design principles for building electric-field-tunable electric devices [6, 7, 15].

Spin-orbit interaction, which entangles the spin and orbital degrees of freedom, plays a key role in many of the proposed hidden spin effects occurring in centrosymmetric crystals with inversion-asymmetric sectors (or sublattices). It is known that spin-orbit coupling (SOC) causes spin splitting in solids lacking an inversion center [16, 17], thereby producing an effective momentum-dependent magnetic field $\Omega(\mathbf{k})$ that couples to spin σ [18, 19]. The crystal space symmetry dictates the specific form of the effective magnetic field as well as the pattern of the corresponding spin texture. Taking a [001]-oriented III-V zinc-blende semiconductor quantum well (QW) with the C_{2v} point group as an example [19, 20], the effective magnetic field of the Dresselhaus effect $\Omega_D(\mathbf{k})$ takes the form of $\lambda_D(k_y, k_x)$, whereas that

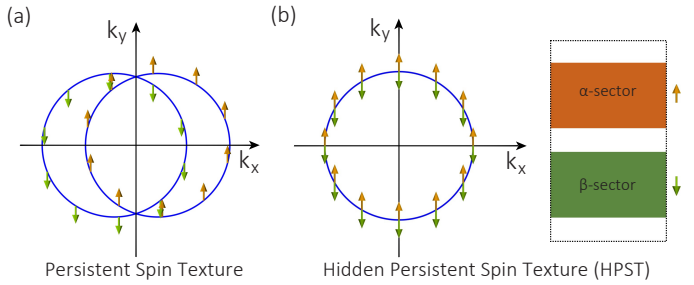


FIG. 1. (a) Persistent spin texture in a QW system with equal magnitudes of Dresselhaus and Rashba parameters. (b) Schematic illustration of HPST in momentum space (left panel) and real space (right panel). Orange and green arrows denote the spin orientations. The black dashed box in (b) indicates the unit cell comprising α - and β -sectors, corresponding to the separated distribution of the two degenerate subband states, respectively.

of Rashba effect $\Omega_R(\mathbf{k})$ is written as $\lambda_R(-k_y, k_x)$, corresponding to a characteristic helical spin texture. Based on the chiral spin textures, kinds of related spin phenomena and spintronics applications are proposed [18], such as spin-Hall conductivity [21, 22], spin-galvanic effect [23], current-induced spin polarization [24], and spin field-effect transistor [25].

Specially, in the case of III-V zinc-blende QW, a momentum-independent spin configuration arises if $\lambda_D = \pm \lambda_R = \lambda/2$, termed as persistent spin texture [26], which stems from a unidirectional effective magnetic field Ω_{PST} described by $\lambda(k_y, 0)$ or $\lambda(0, k_x)$ [27]. As schematically shown in Fig. 1(a), each splitted electronic subband possesses a uniform spin configuration with spin orientation exactly pointing to the $\pm y$ -direction as a result of $\Omega_{PST} = \lambda(0, k_x)$, envisioning a possibility to realize a spatially periodic mode, i.e., persistent spin helix [28]. The unique spin helix state is protected by

* jwluo@semi.ac.cn

the $SU(2)$ spin rotation symmetry and is robust against spin-independent disorder scattering, which is crucial for achieving a long spin lifetime [29]. However, it has only been experimentally confirmed in several semiconductor QW structures [30–33], posing a critical challenge for further research.

Inspired by the discovered hidden Rashba and Dresselhaus effects, one may naturally wonder whether the persistent spin texture could also exist hiddenly in solid-state materials. Such an interesting question has not been explored before. Particularly, the hidden persistent spin texture (HPST) should be an intrinsic property that circumvents the stringent conditions required to satisfy $\lambda_D = \pm \lambda_R$ in QW systems, e.g., the precise control of the QW width, the strength of external electric field and the doping level [26], going beyond the existing design paradigm of persistent spin texture.

In this work, we theoretically demonstrate the existence of HPST in bulk crystals with sublattice structures by using symmetry analysis in conjunction with density-functional theory (DFT) calculations. Figure 1(b) conceptually plots the distribution of HPST states in momentum and real spaces. Compared with conventional persistent spin texture for spin-split states, it exhibits a unique spin-sector locking effect for HPST: the momentum-independent spin orientations of the energy-degenerate states compensate each other in momentum space; additionally, the opposite spins are spatially segregated in different real-space sectors. In such a case, a nonsymmorphic twofold screw-rotational operation acting on the sublattice degree of freedom by connecting the α - to β -sector contributes greatly to the occurrence of HPST, as we will discuss in the following.

HPST in centrosymmetric crystals. We first consider the HPST in nonmagnetic centrosymmetric systems. Consequently, both the space inversion symmetry \mathcal{P} and time-reversal symmetry \mathcal{T} are preserved, and $(\mathcal{PT})^2 = -1$ for a spin-half system, ensuring a (at least) twofold degeneracy for all bands in the Brillouin zone (BZ). The doublet states $(\psi_k, \Theta\psi_k)$ form a Kramers pair, where $\Theta = \mathcal{PT}$. However, this joint operation does not impose enough constraint on the specific form of $\Omega(\mathbf{k})$, so that other symmetry operations are necessitated to guarantee a HPST. This goal can be achieved by a nonsymmorphic symmetry involving a twofold rotation plus a half translation along the rotation axis $S_{2z} : (x, y, z) \rightarrow (-x, -y, z + \frac{1}{2})$ (here the screw axis is taken along z).

We focus on the $k_z = \pi$ plane, and *any* point on this plane is invariant under the combined operation $S_{2z}\mathcal{P}$. Note that $S_{2z}^2 = T_{001} = e^{-ik_z}$, and S_{2z} anticommutes with \mathcal{P} at the whole plane because of $T_{001}\mathcal{P}S_{2z} = S_{2z}\mathcal{P} = e^{-ik_z}\mathcal{P}S_{2z}$, where T_{001} denotes a lattice constant translation along the z -direction. Hence, we obtain $(S_{2z}\mathcal{P})^2 = -1$ at $k_z = \pi$ considering also the spin space, and thus we can label the doublet $(\psi_k, \Theta\psi_k)$ by using the eigenvalues $\pm i$ of $S_{2z}\mathcal{P}$, namely, $S_{2z}\mathcal{P}|\psi_k^{\pm i}\rangle = \pm i|\psi_k^{\pm i}\rangle$ and $S_{2z}\mathcal{P}|\Theta\psi_k^{\pm i}\rangle = \pm i|\Theta\psi_k^{\pm i}\rangle$. As a result, two conju-

gated doublets $(\psi_k^{+i}, \Theta\psi_k^{+i})$ and $(\psi_k^{-i}, \Theta\psi_k^{-i})$ with different $S_{2z}\mathcal{P}$ eigenvalues appear at each point on that plane.

In fact, since $S_{2z}\mathcal{P}$ anticommutes with σ_x and σ_y in the spin space, we have $\langle\psi_k^{+i}|\sigma_{x,y}|\psi_k^{+i}\rangle = \langle\psi_k^{+i}|(S_{2z}\mathcal{P})^{-1}\sigma_{x,y}S_{2z}\mathcal{P}|\psi_k^{+i}\rangle = -\langle\psi_k^{+i}|\sigma_{x,y}|\psi_k^{+i}\rangle$, i.e., $\langle\psi_k^{+i}|\sigma_{x,y}|\psi_k^{+i}\rangle = 0$. A similar analysis results in $\langle\Theta\psi_k^{+i}|\sigma_{x,y}|\Theta\psi_k^{+i}\rangle = 0$, and the same conclusion also applies to the other doublet $(\psi_k^{-i}, \Theta\psi_k^{-i})$. That is to say, the expectation values of spin operators s_x and s_y ($\mathbf{s} = \frac{\hbar}{2}\langle\sigma\rangle$) are forced to be zero within each of the two doublets. By contrast, due to Θ , the z -component spin expectation, s_z , are finite but with opposite orientations within each paired doublet states. In addition, the combination of S_{2z} and \mathcal{T} can realize the wavefunction segregation of such doublet states in separated real-space sectors connected by S_{2z} , as discussed in previous works [6, 15, 34]. Therefore, a symmetry-enforced HPST on the $k_z = \pi$ plane is demonstrated, manifesting a uniform spin configuration pointing to a fixed direction locally in each sector.

To explicitly demonstrate the above point, we carry out a first-principles calculation on the centrosymmetric material WSe₂ [35]. As illustrated in Fig. 2(a), it has a van der Waals layered crystal structure in the space group $P6_3/mmc$ (No. 194) [36], which contains an in-

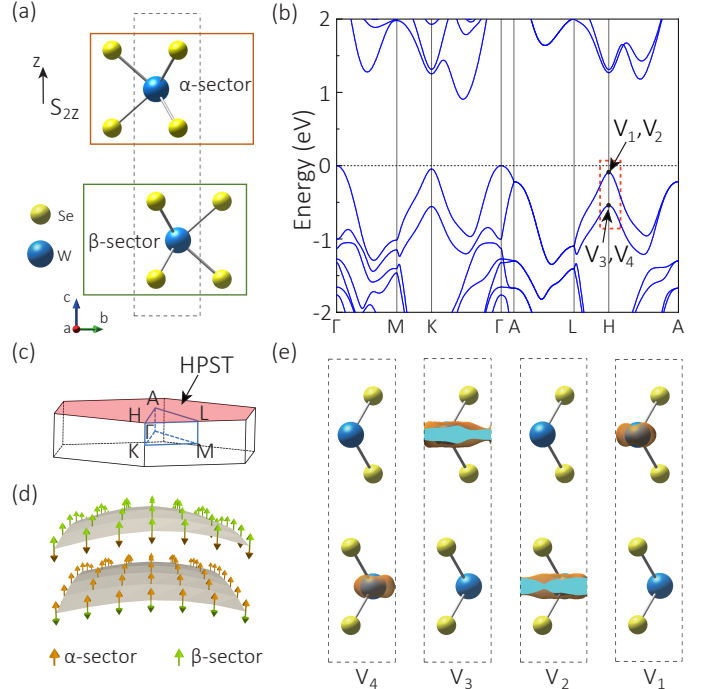


FIG. 2. (a) Crystal structure of centrosymmetric bulk WSe₂, which contains a twofold screw rotation S_{2z} . (b) Band structure in the presence of SOC. (c) The corresponding BZ, where the symmetry-protected HPST is schematically shown by the red shaded surfaces. (d) HPST around H indicated by the red box in (b). (e) Charge density distribution plotted for states V_4, V_3, V_2 and V_1 .

version center and a screw axis S_{2z} . In one unit cell, two sandwich layers, which are related to each other by S_{2z} , are indicated as the α -sector and β -sector. Fig. 2(b) depicts the calculated band structure along the high symmetry lines in the BZ with SOC included, where no spin splitting is observed as expected for centrosymmetric materials. The material has an indirect bandgap of 0.91 eV with the conduction-band minimum (CBM) located on the $K - \Gamma$ path, whereas the valence-band maximum (VBM) is at the Γ point. Besides, one observes that there is a local band maximum located at the H point for the highest occupied valence band, the energy of which is only slightly below the VBM. We mark the two valence-band doublet states at the H point by (V_1, V_2) and (V_3, V_4) , respectively.

According to our previous analysis, there must exist a HPST located at the $k_z = \pi$ plane containing the route $A - L - H - A$, as shown by the red shaded surface in Fig. 2(c). Our first-principles calculation results indeed confirm it [35]. As a typical example, we plot the two-dimensional (2D) band dispersion together with the calculated local spin polarizations in the vicinity of the H point when $k_z = \pi$. It clearly shows that each of the two twofold degenerate band states have finite and opposite spin polarizations, whose orientations are exactly along the z -direction and remain independent of the momentum, mimicking a hidden Zeeman-type spin polarization [15]. Meanwhile, by examining the spatial distribution of the marked doublet states at the H point [see Fig. 2(e)], one finds the following features. (i) The band states are mainly distributed in the two Mo atomic layers. (ii) The charge density distribution of the V_1 state is confined in the α -sector whereas for the V_2 state it is segregated in the β -sector. (iii) The sector distribution pattern is reversed for the other doublet states V_3 and V_4 . Therefore, the first-principles calculation identifies the existence of HPST in WSe₂, consistent with our theory.

HPST in noncentrosymmetric crystals. Is it possible to have HPST hosted in nonmagnetic inversion-asymmetric materials? The first consideration is that the symmetry-protected double degeneracy should be realized on a BZ plane in terms of the definition of HPST. We find the combination of a S_{2z} with the retained \mathcal{T} can meet this objective despite the broken \mathcal{P} . The reason is that the $S_{2z}\mathcal{T}$ operation preserves the k point on the $k_z = \pi$ plane and $(S_{2z}\mathcal{T})^2 = -1$, which can generate Kramers doublet states $(\psi_k, \tilde{\Theta}\psi_k)$, where $\tilde{\Theta} = S_{2z}\mathcal{T}$, and thereby can protect the states on a whole BZ surface with a twofold degeneracy, known as nodal surface states [37–39]. On this basis, we find that the minimal set of symmetries should include another n-fold rotational operation ($n \geq 3$) along the z -direction to enable a HPST appearing around certain high symmetry points (not limited to time-reversal invariant momentum point).

We then illustrate this behavior via a concrete material example—the BaBi₄O₇. It crystallizes in a hexagonal structure with space group P6₃mc (No. 186)[40],

which excludes the inversion center but maintains the S_{2z} . Fig. 3(a) shows the crystal structure of BaBi₄O₇, of which the unit cell can be divided into a pair of sectors (termed as α -sector and β -sector) connected by S_{2z} . The calculated band structure for BaBi₄O₇ in the presence of SOC is plotted in Fig. 3(b). One observes that it is an indirect bandgap semiconductor with a fundamental band gap of 1.71 eV. As expected, the absence of \mathcal{P} generally lifts the band degeneracy in the BZ except for the band states on the $k_z = \pi$ plane, i.e., along the high symmetry lines $A - L - H - A$. This is in agreement with the above argument that the antiunitary symmetry $\tilde{\Theta}$ guarantees a twofold degeneracy on that plane.

Similar to the case of WSe₂, we focus our attention on the high symmetry point H given that the formed valley at this point for the highest valence-band is nearly degenerate to the VBM. The calculated 2D band structure and the corresponding sector-decomposed spin polarization are shown in the inset of Fig. 3(b). Interestingly, we do, on the whole, obtain a HPST-like pattern with a strongly dominant z -component of the spin vector in the BZ. Moreover, we plot the charge density distribution of the hole states indicated by V'_1, V'_2, V'_3, V'_4 around the H point in Fig. 3(c), which share similar features to those of WSe₂, further confirming the emergent HPST in BaBi₄O₇. It is noteworthy that such an unexpected hidden-like spin polarization effect in noncentrosymmetric materials has yet to be reported.

Figures 3(d–e) illustrate the 2D diagrams of the spin polarizations for nodal surface doublet states $(\psi_k, \tilde{\Theta}\psi_k)$ near the H point, where the sampled centers correspond to the states V'_1 and V'_2 , respectively. In comparison with the HPST in centrosymmetric crystals, the main difference lies in that there is an increasing in-plane spin component as the momentum moves away from the H point, which cannot be compensated by its Kramers partner. In contrast, the doublet states have the same in-plane magnitude and orientation of the spin vector. This can be easily understood by the antiunitary symmetry $\tilde{\Theta}$ acting on the spin space. In this process, the \mathcal{T} first transforms the spin components from (s_x, s_y, s_z) to $(-s_x, -s_y, -s_z)$, and then S_{2z} transforms $(-s_x, -s_y, -s_z)$ to $(s_x, s_y, -s_z)$, leading to the opposite out-of-plane spin components but the same in-plane spin components between ψ_k and $\tilde{\Theta}\psi_k$. Additionally, we see that the in-plane spin components $s_{x,y}$ exhibit a helical spin texture with a counterclockwise chirality.

Next, we construct an effective $k \cdot p$ Hamiltonian to further explain the hidden-like spin textures occurring in BaBi₄O₇. The symmetry operations in the little group at H include $S_{2z}\mathcal{T}$, C_{3z} and additionally $\tilde{M}_x : (x, y, z) \rightarrow (-x, y, z + \frac{1}{2})$, with the following matrix representations [41], $S_{2z}\mathcal{T} = i\tau_y \otimes \sigma_x K$, $C_{3z} = \tau_0 \otimes e^{-i\frac{\pi}{3}\sigma_z}$ and $\tilde{M}_x = \tau_y \otimes \sigma_x$. Here, τ and σ are Pauli matrices describing the sublattice and spin spaces, respectively, and K is the complex conjugation. Constrained by these symmetries, the effective Hamiltonian to the lowest order

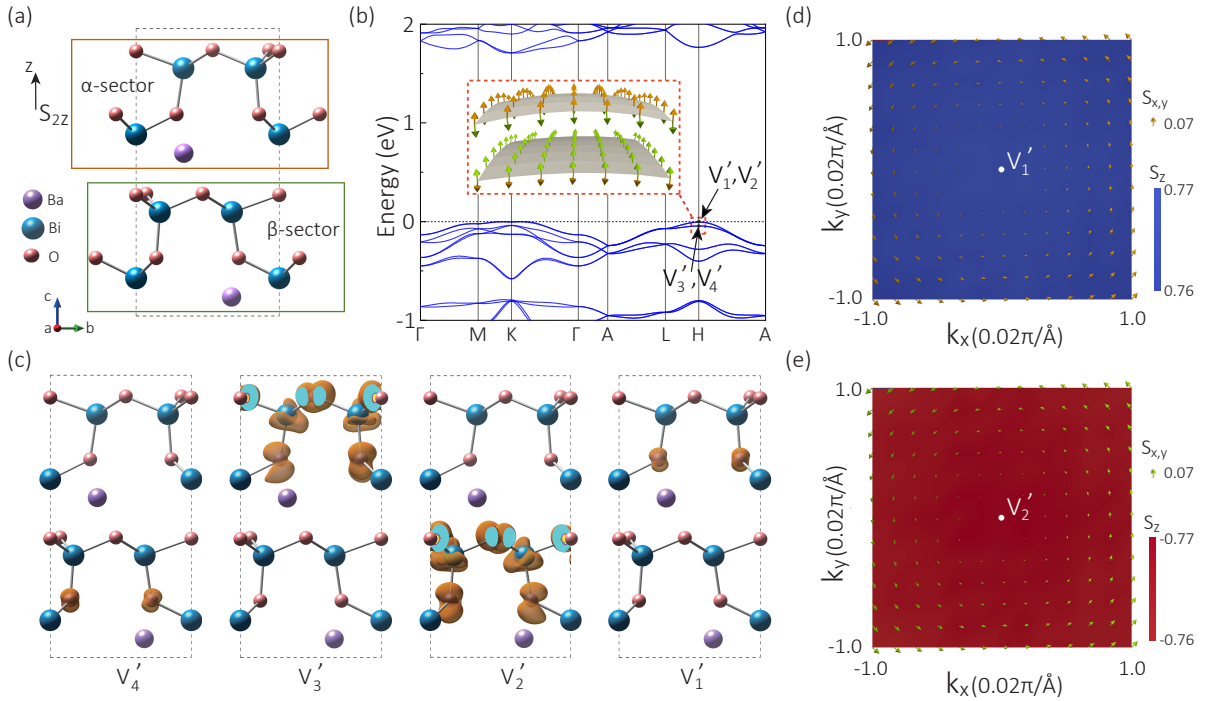


FIG. 3. (a) Crystal structure of non-centrosymmetric BaBi_4O_7 , where the nonsymmorphic S_{2z} is preserved. (b) Band structure for BaBi_4O_7 with SOC. Inset is the 2D plot of HPST around the H point indicated by the red dashed box. (c) Charge density distribution plotted for states V'_4 , V'_3 , V'_2 and V'_1 . 2D plot of spin patterns for (d) V'_1 and (e) V'_2 , respectively. The in-plane spin components s_x and s_y , are represented by the arrows whereas the out-of-plane spin component s_z is shown by color.

expanded around H is given by

$$\mathcal{H}(\mathbf{k}) = \alpha(k_y\sigma_x - k_x\sigma_y) + M\tau_z \otimes \sigma_z - \beta k_z\tau_y \otimes \sigma_0, \quad (1)$$

where M , α , and β are constants, and the wave vector \mathbf{k} is referenced with respect to the H point. The band energies of Eq. 1 read $E(\mathbf{k}) = \pm\sqrt{M^2 + (\alpha k_{\parallel} \pm \beta k_z)^2}$, where $k_{\parallel} = \sqrt{k_x^2 + k_y^2}$.

For $k_z = 0$, the Hamiltonian (1) is reduced to $\mathcal{H}(k_{\parallel}) = \alpha(k_y\sigma_x - k_x\sigma_y) + M\tau_z \otimes \sigma_z$. One finds that there emerge two doublets with degenerate energies $E^{\pm}(k_{\parallel}) = \pm\sqrt{M^2 + (\alpha k_{\parallel})^2}$, yielding nodal surface states on the BZ boundary. Furthermore, the Hamiltonian now can be easily diagonalized in the sublattice space due to its commutativity with the sector measurement operator $\tau_z \otimes \sigma_0$. We then obtain an equivalent effective magnetic field $\mathbf{\Omega}(\mathbf{k})$ taking the form of $(\alpha k_y, -\alpha k_x, \eta M)$, which has the opposite sign of the z-component for different sectors, i.e., the values of $\eta = \pm 1$. Accordingly, the expectation values of the spin operator for the two doublet states are calculated to be

$$(s_x, s_y, s_z)_{\eta}^{\pm} = \pm \frac{\hbar}{2\sqrt{M^2 + (\alpha k_{\parallel})^2}} (-\alpha k_y, \alpha k_x, \eta M). \quad (2)$$

Hence, there exists a totally compensated z-component of spin vector for one doublet exactly at H (when $k_{\parallel} = 0$), which is in line with the DFT calculations. The evaluated parameters by fitting the calculation results are M

$= 0.02$ eV and $\alpha = 0.031$ eV \AA . As a result, the in-plane spin components in the vicinity of H point are negligible compared with its z-component, exhibiting a nearly HPST that covers a large portion of the BZ. The range of k_x and k_y values in Figs. 3(d-e) spans $0.04\pi \text{\AA}^{-1}$ around H, comparable to the values proposed in BiInO_3 with conventional persistent spin texture [27]. This makes BaBi_4O_7 ideal for studying HPST in noncentrosymmetric materials.

Discussion. We have uncovered the HPST in both centrosymmetric and non-centrosymmetric bulk materials, where the nonsymmorphic symmetry plays a crucial role. As discussed above, the screw axis has been assumed along z in centrosymmetric systems, which can display a HPST at $k_z = \pi$ with an out-of-plane spin configuration due to the combined operation $S_{2z}\mathcal{P}$. In fact, this combined operation corresponds to a glide mirror operation $\widetilde{M}_x : (x, y, z) \rightarrow (x, y, -z + \frac{1}{2})$. Similarly, if we have a screw axis along the direction x or y , a HPST at $k_x = \pi$ or $k_y = \pi$ can be realized.

We point out that the presence of HPST discussed in centrosymmetric crystals is solely determined by symmetry, and its location is fixed at the BZ boundary plane. For this reason, the essentially symmetry-enforced HPST is independent of the specific material, making it easier for the exploration of candidate materials by analyzing the space groups with an inversion center [42]. By contrast, for noncentrosymmetric materials, the S_{2z} can guarantee a HPST only around certain high-symmetry

points in BZ, and the size of the region displaying an approximate HPST is much related to the detailed material properties. Nevertheless, our results on BaBi_4O_7 serve as an important first step towards this goal.

We propose that the HPST behavior revealed in WSe_2 and BaBi_4O_7 can be directly probed via nuclear magnetic resonance measurements [43] or spin- and angle-resolved photoemission spectroscopy [3–5], analogous to experimental detection of the hidden Rashba and Dresselhaus effects. Particularly, our proposed HPST here is gauge-invariant since the choice of sectors is definite thanks to the nontrivial protection of wavefunction segregation by S_{2z} [6, 15, 44].

We may expect interesting properties for states around HPST such as the large anisotropic g-factor arising from the characteristic pattern of effective magnetic field locked to a unique direction in centrosymmetric crystals.

In addition, for HPST in non-centrosymmetric materials, an enhanced mobility along the z -direction is also expected because of the suppressed backscattering from scatterers that preserve the spin.

ACKNOWLEDGMENTS

This work is supported by the National Key Research and Development Program of China (Grant No. 2018YFB2202800), the National Natural Science Foundation of China (Grant No. 11904359), and the Strategic Priority Research Program of Chinese Academy of Sciences (Grant No. XDB30000000). J.W.L. is supported by the National Natural Science Foundation of China (Grants No. 61888102 and No. 11925407), and the National Key Research and Development Program of China (Grant No. 2018YFB2200105).

-
- [1] X. Zhang, Q. Liu, J.-W. Luo, A. J. Freeman, and A. Zunger, *Nature Physics* **10**, 387 (2014).
- [2] B. Partoens, *Nature Physics* **10**, 333 (2014).
- [3] J. M. Riley, F. Mazzola, M. Dendzik, M. Michiardi, T. Takayama, L. Bawden, C. Granerd, M. Leandersson, T. Balasubramanian, M. Hoesch, T. K. Kim, H. Takagi, W. Meevasana, P. Hofmann, M. Bahramy, J. Wells, and P. C. King, *Nature Physics* **10**, 835 (2014).
- [4] S.-L. Wu, K. Sumida, K. Miyamoto, K. Taguchi, T. Yoshikawa, A. Kimura, Y. Ueda, M. Arita, M. Nagao, S. Watauchi, I. Tanaka, and T. Okuda, *Nature Communications* **8**, 1919 (2017).
- [5] W. Yao, E. Wang, H. Huang, K. Deng, M. Yan, K. Zhang, K. Miyamoto, T. Okuda, L. Li, Y. Wang, H. Gao, C. Liu, W. Duan, and S. Zhou, *Nature Communications* **8**, 14216 (2017).
- [6] L. Yuan, Q. Liu, X. Zhang, J.-W. Luo, S.-S. Li, and A. Zunger, *Nature Communications* **10**, 906 (2019).
- [7] Z. Lin, C. Wang, Y. Xu, and W. Duan, *Phys. Rev. B* **102**, 165143 (2020).
- [8] Q. Liu, X. Zhang, and A. Zunger, *Phys. Rev. Lett.* **114**, 087402 (2015).
- [9] J. H. Ryoo and C.-H. Park, *NPG Asia Materials* **9**, e382 (2017).
- [10] S. Cho, J.-H. Park, J. Hong, J. Jung, B. S. Kim, G. Han, W. Kyung, Y. Kim, S.-K. Mo, J. D. Denlinger, J. H. Shim, J. H. Han, C. Kim, and S. R. Park, *Phys. Rev. Lett.* **121**, 186401 (2018).
- [11] C.-X. Liu, *Phys. Rev. Lett.* **118**, 087001 (2017).
- [12] K. Gotlieb, C.-Y. Lin, M. Serbyn, W. Zhang, C. L. Smallwood, C. Jozwiak, H. Eisaki, Z. Hussain, A. Vishwanath, and A. Lanzara, *Science* **362**, 1271 (2018).
- [13] Z.-M. Yu, S. Guan, X.-L. Sheng, W. Gao, and S. A. Yang, *Phys. Rev. Lett.* **124**, 037701 (2020).
- [14] J.-L. Zhang, Y. Li, W. Huang, and F.-C. Zhang, *Phys. Rev. B* **102**, 180509 (2020).
- [15] S. Guan and J.-W. Luo, *Phys. Rev. B* **102**, 184104 (2020).
- [16] G. Dresselhaus, *Phys. Rev.* **100**, 580 (1955).
- [17] Y. A. Bychkov and E. I. Rashba, *JETP Lett.* **39**, 78 (1984).
- [18] A. Manchon, H. C. Koo, J. Nitta, S. M. Frolov, and R. A. Duine, *Nature Materials* **14**, 871 (2015).
- [19] R. Winkler, *Spin-Orbit Coupling Effect in Two-Dimensional Electron and Hole Systems* (Springer, 2003).
- [20] L. L. Tao, T. R. Paudel, A. A. Kovalev, and E. Y. Tsymbal, *Phys. Rev. B* **95**, 245141 (2017).
- [21] J. E. Hirsch, *Phys. Rev. Lett.* **83**, 1834 (1999).
- [22] S. Zhang, *Phys. Rev. Lett.* **85**, 393 (2000).
- [23] S. D. Ganichev, E. L. Ivchenko, V. V. Bel'kov, S. A. Tarasenko, M. Sollinger, D. Weiss, W. Wegscheider, and W. Prettl, *Nature* **417**, 153 (2002).
- [24] V. Edelstein, *Solid State Communications* **73**, 233 (1990).
- [25] S. Datta and B. Das, *Applied Physics Letters* **56**, 665 (1990).
- [26] J. Schliemann, *Rev. Mod. Phys.* **89**, 011001 (2017).
- [27] L. L. Tao and E. Y. Tsymbal, *Nature Communications* **9**, 2763 (2018).
- [28] B. A. Bernevig, J. Orenstein, and S.-C. Zhang, *Phys. Rev. Lett.* **97**, 236601 (2006).
- [29] M. Kammermeier, P. Wenk, and J. Schliemann, *Phys. Rev. Lett.* **117**, 236801 (2016).
- [30] J. D. Koralek, C. P. Weber, J. Orenstein, B. A. Bernevig, S.-C. Zhang, S. Mack, and D. D. Awschalom, *Nature* **458**, 610 (2009).
- [31] M. P. Walser, C. Reichl, W. Wegscheider, and G. Salis, *Nature Physics* **8**, 757 (2012).
- [32] M. Kohda, V. Lechner, Y. Kunihashi, T. Dollinger, P. Olbrich, C. Schönhuber, I. Caspers, V. V. Bel'kov, L. E. Golub, D. Weiss, K. Richter, J. Nitta, and S. D. Ganichev, *Phys. Rev. B* **86**, 081306 (2012).
- [33] A. Sasaki, S. Nonaka, Y. Kunihashi, M. Kohda, T. Bauernfeind, T. Dollinger, K. Richter, and J. Nitta, *Nature Nanotechnology* **9**, 703 (2014).
- [34] Y. Zhang, P. Liu, H. Sun, S. Zhao, H. Xu and Q. Liu, *Chinese Physics Letters* **37**, 087105 (2020).
- [35] See the Supplemental Material at <http://link.aps.org/> for details of the first-principles calculation, and the calculated hidden persistent spin texture for WSe_2 at the

- $k_z = \pi$ BZ plane .
- [36] R. Coehoorn, C. Haas, J. Dijkstra, C. J. F. Flipse, R. A. de Groot, and A. Wold, *Phys. Rev. B* **35**, 6195 (1987).
- [37] C. Zhong, Y. Chen, Y. Xie, S. A. Yang, M. L. Cohen, and S. B. Zhang, *Nanoscale* **8**, 7232 (2016).
- [38] Q.-F. Liang, J. Zhou, R. Yu, Z. Wang, and H. Weng, *Phys. Rev. B* **93**, 085427 (2016).
- [39] W. Wu, Y. Liu, S. Li, C. Zhong, Z.-M. Yu, X.-L. Sheng, Y. X. Zhao, and S. A. Yang, *Phys. Rev. B* **97**, 115125 (2018).
- [40] L. Klinkova, V. Nikolaichik, L. Zorina, N. Barkovskii, V. Fedotov, and A. Zver'Kov, *Zhurnal Neorganicheskoy Khimii* **41**, 709 (1996).
- [41] C. J. Bradley and A. P. Cracknell, *The Mathematical Theory of Symmetry in Solids* (Clarendon, Oxford, 1972).
- [42] M. I. Aroyo, J. M. Perez-Mato, C. Capillas, E. Kroumova, S. Ivantchev, G. Madariaga, A. Kirov, and H. Wondratschek, *Zeitschrift fr Kristallographie - Crystalline Materials* **221**, 15 (2006).
- [43] J. Ramírez-Ruiz, S. Boutin, and I. Garate, *Phys. Rev. B* **96**, 235201 (2017).
- [44] P. Li and I. Appelbaum, *Phys. Rev. B* **97**, 125434 (2018).